

Simulation of Fatigue Fracture Propagation in Concrete using a Lattice Model

Andrea Carpinteri^{1,a}, Andrea Spagnoli^{1,b}, Li-Ping Guo^{2,c}, Sabrina Vantadori^{1,d}

¹Department of Civil-Environmental Engineering and Architecture, University of Parma, Italy

²College of Materials Science and Engineering, Southeast University, Nanjing, China

^aandrea.carpinteri@unipr.it, ^bspagnoli@unipr.it,
^cguoliping691@163.com, ^dsabrina.vantadori@unipr.it

Keywords: Concrete; Fatigue damage; Fracture propagation; Lattice model; Material meso-structure.

Abstract. The fracture propagation in concrete under fatigue loading is analysed using a two-dimensional lattice model. A regular triangular lattice model (formed by pin-joined truss elements) accounting for the actual multiphase structure (at the meso-scale level) of the material is developed (an automatic image processing procedure for phase detection is adopted). The properties of each truss in the lattice are assigned according to the phase (coarse aggregate, mortar matrix, air bubble, mortar-aggregate interface) the truss lies over. Under monotonic loading, the trusses are assumed to have a linear elastic behavior in compression, whereas in tension a linear elastic behavior up to a certain peak load is followed by a linear softening branch. Fatigue damage is accounted for by considering a suitable elastic stiffness degradation. Some numerical results related to high-performance concrete specimens under high-cycle bending loading are presented.

Introduction

The fracture behavior up to failure of quasi-brittle materials like concrete is strongly affected by the micromechanical mechanisms developing in the heterogeneous microstructure of the material. A large amount of research has been carried out in order to simulate such a material behavior using realistic but simplified models of the multiphase microstructure (e.g. see Ref. [1]). Among others, following the early so-called framework method of Hrennikoff [2] to simulate elasticity problems, the lattice models have been developed to analyse concrete fracture [3-5]. Accordingly the continuum model of the material is substituted by an array of discrete elements forming a truss or a frame structure; the multiphase characteristic of the material is simulated by assigning different mechanical properties to the truss/beam elements of the lattice model.

Since a great deal of research work performed by using 2D/3D lattice models is based on assumed cracks or artificially disordered microstructures constituted by idealized circular aggregates [6], the simulation results cannot exactly reflect the actual fracture patterns in real concrete structural components. To overcome this problem, digital image-based models have been introduced (e.g. see Refs [7,8]) to describe the actual microstructure of the material and in turn to perform a realistic simulation of fracture propagation in concrete. To the authors' best knowledge, all published research achievements using lattice models are related to monotonic loads, while the concrete behaviour under cyclic loads has not yet been examined through the lattice model. Some theoretical approaches, not based on lattice models, for describing the fatigue behavior of concrete can be found for instance in Refs [9,10].

In the present paper, the fracture propagation in concrete under fatigue loading is analysed using a two-dimensional lattice model. A regular triangular lattice model (formed by pin-joined truss elements) accounting for the actual multiphase structure (at the meso-scale level) of the material is developed, and an automatic image processing procedure for phase detection is adopted. The

properties of each truss in the lattice are assigned according to the phase (coarse aggregate, mortar matrix, air bubble, mortar-aggregate interface) the truss lies over. Under monotonic loading, the trusses are assumed to have a linear elastic behavior in compression, whereas in tension a linear elastic behavior up to a certain peak load is followed by a linear softening branch. Fatigue damage is accounted for by considering a suitable elastic stiffness degradation. Some numerical results related to high-performance concrete specimens under high-cycle bending loading are presented.

Brief Description of the Lattice Model

General Features. A two-dimensional lattice is adopted to discretize the continuum model of the material. A regular triangular lattice (having hexagonal unit cells) with truss (spring) elements is used. The length l of the truss elements dictates the level of the discretization (Fig. 1).

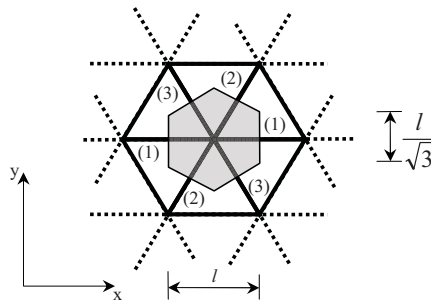


Figure 1. The unit cell of a regular triangular lattice.

For the modeling of material heterogeneities (at the desired micro-/meso-level), different mechanical properties are assigned to the lattice elements to describe the different components (coarse aggregate, mortar matrix, air bubble) of the material (which is hence treated as an n -phased composite material). This requires to identify the regions occupied by these components (the identification procedure is described in the following).

The above model is run through the finite element code ABAQUS using the UMAT subroutine for implementing the constitutive law and the fatigue damage evolution law. Cyclic loads are applied under stress control through a sequence of blocks of loading cycles with constant amplitude. A step-by-step non-linear procedure, based on a secant stiffness matrix approach, is employed, where each step corresponds to a load reversal.

Elastic Behavior. The Young modulus of the truss elements in the lattice determines the stiffness of the continuum discretized through the lattice. The relationship between the Young modulus (\bar{E}_0) of the truss and that (E_0) of the continuum can be obtained by equating the elastic strain energy of the continuum occupying an hexagonal unit cell (having unit thickness) with that of the lattice occupying the same region (Fig. 1) [11], namely:

$$\bar{E}_0 = \frac{\sqrt{3}l}{2A} E_0 \tag{1}$$

where A is the cross section area of the truss element. From now onwards we adopt the following notation: a bar above the symbol means that the quantity is related to truss elements of the lattice, whereas the plane symbol means that the quantity is related to the continuum. The adopted lattice of truss elements, in contrast with that of beam elements, is computationally less expensive (2 degrees

of freedom per node instead of 3 are present), but we underline that it has the limitation of enforcing a Poisson ratio of the continuum equal to 1/3 [3]. Note that a regular triangular lattice with spatially homogeneous properties produces an overall isotropic behavior.

To switch from continuum to lattice, and hence to be able for instance to describe the constitutive law of the truss elements on the basis of that of the continuum (see below), a transformation rule for stresses has to be adopted. We consider here a plane stress field acting in the continuum (having the 3 components $\sigma_x, \sigma_y, \tau_{xy}$ in the xy frame). Assuming that the lattice unit cell is small enough by size to be regarded as embedded in a uniform stress/strain field, we can write in a compact form (Einstein summation rule is used) [11]:

$$\bar{\sigma}^{(t)} = \bar{E}_0 n_i^{(t)} n_j^{(t)} \varepsilon_{ij} \quad (2)$$

where the index $t = 1, 2, 3$ identifies the truss orientation with respect to the xy frame (Fig. 1), the indexes $i, j = 1, 2$ identify the coordinate axes (1 is for x-axis, 2 for y-axis) so that $\varepsilon_{11} = \varepsilon_x$, $\varepsilon_{22} = \varepsilon_y$, $\varepsilon_{12} = \varepsilon_{21} = \gamma_{xy}/2$, and $n_i^{(t)}$, $n_j^{(t)}$ are the direction cosines of the truss element (t) with respect to the xy frame ($n_1^{(1)} = 1, n_2^{(1)} = 0$; $n_1^{(2)} = 1/2, n_2^{(2)} = \sqrt{3}/2$; $n_1^{(3)} = -1/2, n_2^{(3)} = \sqrt{3}/2$).

If we express the strain components in Eq. 2 as a function of the stress components in the continuum using the generalized Hooke's law (where the Lamé's constants are equal to $[(\sqrt{3}A)/(4l)]\bar{E}_0$), the following relationship between the stress $\bar{\sigma}^{(t)}$ in the truss (t) and the general plane stress tensor can be derived:

$$\begin{Bmatrix} \bar{\sigma}^{(1)} \\ \bar{\sigma}^{(2)} \\ \bar{\sigma}^{(3)} \end{Bmatrix} = \frac{l}{A} \begin{bmatrix} \sqrt{3}/2 & -\sqrt{3}/6 & 0 \\ 0 & \sqrt{3}/3 & 1/2 \\ 0 & \sqrt{3}/3 & -1/2 \end{bmatrix} \begin{Bmatrix} \sigma_x \\ \sigma_y \\ \tau_{xy} \end{Bmatrix} \quad (3)$$

Constitutive Law. The truss elements are assumed to be perfectly elastic in compression, whereas the tensile behavior is elastic up to a peak stress \bar{f}_t followed by a linear softening branch (Fig. 2). The unloading path in the softening range is assumed to pass through the reference system origin. The values of Young modulus in compression and in tension are assumed to be equal to each other. Now, under uniaxial stress condition, the stress in the truss parallel to the loading axis is equal to $\bar{\sigma} = [l\sqrt{3}/(2A)]\sigma$ (e.g. see in Eq. 3 the stress in the truss (1) when x is the loading axis). Accordingly, the tensile strength \bar{f}_t of the truss is assumed to be equal to $[l\sqrt{3}/(2A)]f_t$, where f_t is the tensile strength in the continuum. Obviously, the strain $\bar{\varepsilon}_{el,0}$ of the truss at the elastic limit is equal to \bar{f}_t/\bar{E}_0 .

The ultimate strain $\bar{\varepsilon}_u$ of the truss can be calculated from its fracture energy \bar{G}_f . As a matter of fact, in line with the cohesive crack models, the area under the $\sigma - w$ (stress against crack opening) curve (characterized by a tensile strength f_t and an ultimate crack opening w_u) is equal to the fracture energy. This concept can be translated to the truss elements of the lattice. If the ultimate crack opening \bar{w}_u of the truss is taken to be equal to $\bar{\varepsilon}_u l$, for a linear stress-crack opening curve (see Fig. 2) we have:

$$\bar{\varepsilon}_u = 2 \frac{\bar{G}_f}{\bar{f}_t l} \quad (4)$$

The fracture energy in the truss elements can be determined from the continuum counterpart by considering the influence area, equal to $l/\sqrt{3}$, assigned to a truss submitted to a uniaxial stress along its direction (e.g. see the truss (1) in Fig. 1, submitted to the uniaxial stress σ_x), namely:

$$\bar{G}_f = \frac{l}{A\sqrt{3}} G_f \tag{5}$$

If, at a certain load step, the tensile strain $\bar{\epsilon}$ in the truss is higher than $\bar{\epsilon}_{el,0}$, an iterative procedure up to convergence is performed using a secant stiffness approach.

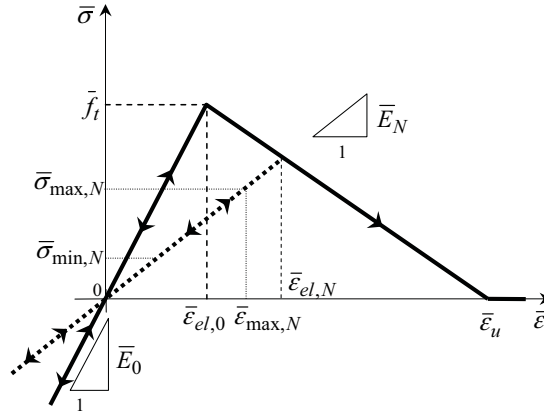


Figure 2. The constitutive law of truss elements of the lattice.

Fatigue Damage Law. We consider a fatigue damage in the truss submitted to cyclic tensile stress. The fatigue damage is regarded as producing an elastic stiffness degradation (Fig. 2). Hence:

$$\bar{E}_N = (1 - D)\bar{E}_0 \tag{6}$$

where \bar{E}_N is the Young modulus after N loading cycles, \bar{E}_0 is the initial Young modulus calculated according to Eq. 1, and D is a damage parameter ranging from 0 (no damage) to 1 (full damage). In the following, we refer to a fatigue damage in the high-cycle regime, that is, a damage caused by stress levels which are below the tensile strength.

A linear damage evolution law is considered [12]:

$$\frac{dD}{dN} = a \left(\frac{\bar{\sigma}_{max,N}(1-R)}{\bar{f}_t} \right)^m \tag{7}$$

where $\bar{\sigma}_{max,N}(1-R)$ is the stress range $\Delta\bar{\sigma}_N$ ($\Delta\bar{\sigma}_N = \bar{\sigma}_{max,N} - \bar{\sigma}_{min,N}$) in the truss during the N -th load cycle (since the behavior is linear in the unloading path, the expression $\bar{\sigma}_{min,N} = \bar{\sigma}_{max,N}R$ holds, where R is the load ratio of the applied loads). The positive constants a and m are material parameters which need to be identified from fatigue experimental data.

Note that the elastic stiffness of every truss element where $\bar{\epsilon}_{max,N} \leq \bar{\epsilon}_{el,N}$ (see the symbols in Fig. 2) is updated at the beginning of each block of loading cycles, by considering a finite increment

of the damage parameter ΔD computed according to Eq.7 for a number ΔN of loading cycles in one block. If $\bar{\epsilon}_{\max, N} > \bar{\epsilon}_{el, N}$, the same iterative procedure described above in relation to $\bar{\epsilon}_{el, 0}$ is used.

Modeling of Material Heterogeneity at the Meso-Level. The modeling of material heterogeneities is carried out following an automatic procedure. In this way the actual material microstructure at the meso-scale level can be modelled. Firstly, a digital image of a cross section of the material specimen is captured. Then, an image processing procedure (an in-house MATLAB program has been developed for this purpose) is applied to the digital images. The procedure allows an automatic detection of different regions characterized by a certain gray level in the digital images, where each region corresponds to a different material phase. At the meso-scale level three phases in the concrete material can be identified: mortar (cement past or matrix), coarse aggregates, voids of entrapped air. Then, a regular triangular lattice is laid over the processed images so that different mechanical properties are attributed to each truss element of the lattice depending on the region (phase) into which the element is located. When a truss element crosses the boundary of a phase region (aggregate/matrix or i -th aggregate/ j -th aggregate), the truss is regarded as an interface element. If the boundary is of the type i -th void/ j -th void, void/matrix, or void/aggregate, the truss is regarded as a void element.

Simulations of Four-Point-Bend Tests

Here we discuss four-point bend tests of plain concrete under fatigue loading. The central part of the specimen (where the bending moment is constant) is discretized using the lattice model presented above. The two sides of the specimen are discretized using elastic 4-node plane stress elements; the purpose of these sides is to transfer the load. Multi-point constraints are employed to ensure the compatibility between the central part (lattice) and the two sides (continuum). The distances between supports and loads are equal to 100mm, and the load span and beam height are nominally equal to 100mm (the actual dimensions might be different from the nominal ones because, in the digital image processing, the external parts of the material microstructure image are disregarded due to their poor quality).

A high-performance concrete is analysed. The ratio of cement:sand:aggregate:water in the concrete mix is 1:1.5:2.4:0.25 by weight (the corresponding nominal volume fraction of aggregate is about 38%). The aggregate is crushed basalt of size range 5-20mm. The sand is siliceous river sand passing through 5-mm sieve. Type II Portland cement with superplasticizer admixture (5kg/m^3) is used. After 90-day curing, the mean compression strength of cubic specimens is equal to 96.5MPa. The Young modulus is equal to 47GPa and the Poisson ratio to 0.2. The bending strength is equal to 9.9MPa and the fracture energy to 308 J/m^2 .

Four types of truss elements are considered in the lattice model to describe: mortar, aggregates, mortar-aggregate interfaces, voids. The relevant mechanical characteristics of the mortar and mortar-aggregate interface are experimentally determined. The Young modulus of the mortar, E_0 , is equal to 83GPa. The tensile strength f_t (measured from bending tests) is equal to 16MPa and 4MPa for mortar and interface, respectively. The fracture energy G_f is equal to 110J/m^2 and 42J/m^2 for mortar and interface, respectively. For the basalt aggregates, typical values taken from the literature are considered ($E_0 = 160\text{GPa}$, $f_t = 22\text{MPa}$ and $G_f = 336\text{J/m}^2$). A case where the tensile strength of the mortar-aggregate interface is 25% higher than the real one (5MPa instead of 4MPa), the other parameters being the same, is also hereafter analysed.

The digital image of the material microstructure shown in Fig. 3 is considered to generate the lattice model. The volume fraction of aggregate is about 42%, whereas the volume fraction of voids is lower than 1% (such values are calculated from the generated lattice model by considering the fraction of the number of truss elements related to aggregates divided by the total number of truss

elements). The load span is equal to 99mm, whereas the beam height is equal to 97mm. The lattice element length l is taken to be equal to 1mm, which is deemed to be a sufficiently small length for the required accuracy (the condition proposed in Ref. [13] $l \leq (1/3)d_{\min}$, where d_{\min} = minimum aggregate size- 5mm in the mix under study, is fulfilled). An estimated value of the specific surface of aggregates is $25\text{cm}^2/\text{cm}^3$ (such a value is estimated from the generated lattice model by considering the ratio between the number of truss elements related to interfaces multiplied by the truss element length l and the calculated total area of the aggregates).

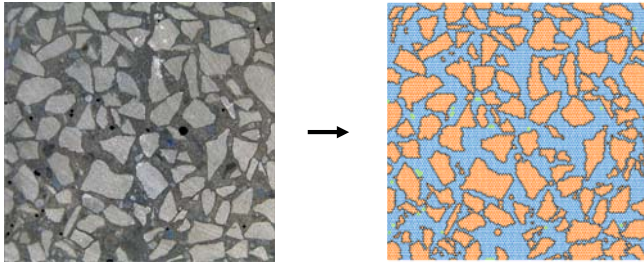


Figure 3. The analysed microstructure of concrete: (left) digital image; (right) lattice model: aggregates (orange), interfaces (black), mortar (blue), voids (green).

The cross section area A of the truss elements is taken as equal to unity. The nominal ultimate bending moment is equal to 15.5kNm (calculated as the nominal bending strength, 9.9MPa, multiplied by the section modulus of the beam). Cyclic loads with maximum bending moment equal to 70% and 50% of the ultimate bending moment (corresponding fatigue stress level of 0.7 and 0.5, respectively) are considered. The load ratio is taken as equal to zero.

By using Eqs 1 to 5, the above material parameters for the continuum are transformed to the truss counterparts. The voids are modeled using truss elements having a perfectly elastic behavior with a negligible value of Young modulus. The elastic sides for load transfer have a linear elastic behavior with Young modulus equal to 47GPa and Poisson ratio of 0.3 (this is to be consistent with the value for the lattice model which is forced to be 1/3 when truss elements, as in the present case, are used). The value of m is assumed to be equal to 10, which corresponds to the typical value of the inverse slope of a SN curve for concrete in the high-cycle regime. The value of the parameter a has been identified so as to obtain, for fatigue stress level of 0.7, a collapse of the specimen with $f_t = 4\text{MPa}$ at the mortar-aggregate interface after about 100,000 cycles, which is the fatigue life observed experimentally for such a stress level. The parameter a turns out to be equal to 5.5×10^3 . The number of cycles per block (ΔN) is taken as equal to 5,000.

A sample of the evolution of the mid-span deflection (measured at the bottom of the lattice model) with the number of fatigue cycles N (normalized with respect to the number of cycles to failure N_f) is shown in Fig. 4. Failure condition is clearly indicated by the sudden increase in such a deflection. For fatigue stress level of 0.7, the predicted number of load cycles to failure (conventionally measured as a drop of bending stiffness of the beam higher than 90%) is 102,500 and 2,212,500 for tensile strength f_t at the interface equal to 4MPa and 5MPa, respectively (note the remarkable influence of the strength at the mortar-aggregate interface on the fatigue life). For fatigue stress level of 0.5, no failure is predicted in the simulations after 2,250,000 load cycles (note that this run-out result is also observed in the experiments, where $f_t = 4\text{MPa}$ at the interface).

The fatigue fracture propagation at incipient failure is illustrated by the deformed meshes in Fig.5 for fatigue stress level equal to 0.7. The patterns of the dominant fatigue crack leading to failure are clearly visible. Finally we report in Fig. 6 the contours of the damage parameter D at different

fractions of the fatigue life N_f for the interface with $f_t = 4\text{MPa}$. The evolution of the damage is well depicted by these contours; by looking at the material microstructure depicted in Fig. 3, it can be seen that damage evolves preferably along the interfaces between aggregates and mortar.

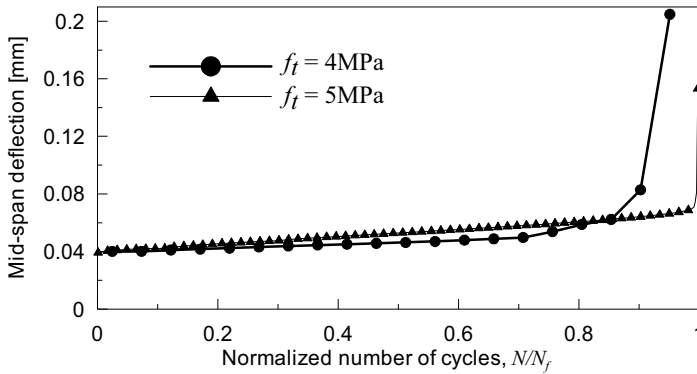


Figure 4. Maximum mid-span deflection against normalized number of cycles for the interface with $f_t = 4\text{MPa}$ and with $f_t = 5\text{MPa}$ under fatigue stress level of 0.7.

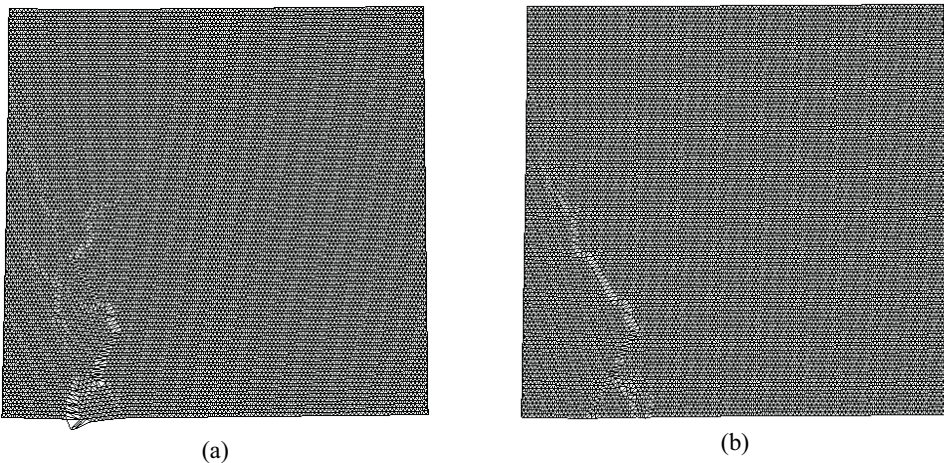


Figure 5. Deformed mesh at incipient failure under fatigue stress level of 0.7 (magnification x10):
(a) $f_t = 4\text{MPa}$ at the interface; (b) $f_t = 5\text{MPa}$ at the interface.

Conclusions

A lattice model to investigate the fatigue fracture propagation in concrete and to predict fatigue life is presented. In the model, the heterogeneity of concrete is described by overlaying digital images of the material microstructure on the lattice. The novelty of the present study is the use of a lattice model for concrete to analyse its fatigue behaviour. The simulations of four-point bend tests demonstrate good prediction capability of the model. Further work is required to validate the model and to offer a numerical tool with good quantitative prediction capabilities.

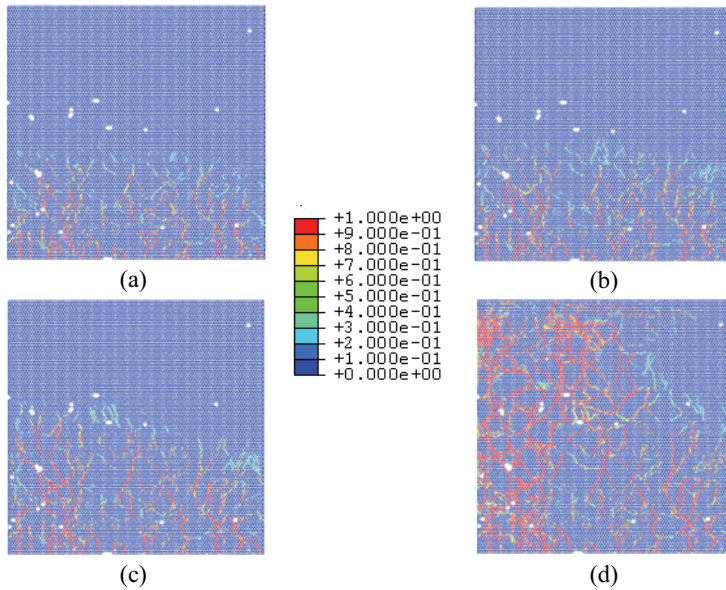


Figure 6. Contour of the damage parameter D at different number of cycles for $f_t = 4\text{MPa}$ at the interface under fatigue stress level of 0.7: (a) $0.4 N_f$; (b) $0.6 N_f$; (c) $0.8 N_f$; (d) N_f .

References

- [1] Z.P. Bazant and J. Planas: *Fracture and Size Effect in Concrete and Other Quasibrittle Materials* (CRC Press, Boca Raton, USA, 1998)
- [2] A. Hrennikoff: *J. Appl. Mech.* Vol. 12 (1941), pp. 169-175
- [3] E. Schlangen and J.G.M. van Mier: *Maters & Structures* Vol. 25 (1992), pp. 534-542
- [4] E. Schlangen and E.J. Garboczi: *Engng Fract. Mechs* Vol. 57 (1997), pp. 319-332
- [5] G. Lilliu and J.G.M. van Mier: *Engng Fract. Mechs* Vol. 70 (2003), pp. 927-941
- [6] J.P.B. Leite, V. Slowik and H. Mihashi: *Cement Concrete Res.* Vol. 34 (2004), pp. 1025-1033
- [7] K. Terada, T. Miura and N. Kikuchi: *Comput. Mechs* Vol. 20 (1997), pp. 331-346
- [8] M. Asai, K. Terada and K. Ikeda, in: *Fracture Mechanics of Concrete Structures*, edited by de Borst et al, Swets & Zeitlinger Press, Lisse, pp. 757-764 (2001)
- [9] T. Matsumoto and V.C. Li: *Cement Concrete Comp.* Vol. 21 (1999), pp. 249-261
- [10] A. Carpinteri, A. Spagnoli and S. Vantatori: *Int. J. Solids Structures* Vol. 43 (2006), pp. 4917-4936
- [11] M. Ostoja-Starzewski: *Applied Mechanics Rev.* Vol. 55 (2002), pp. 38-40
- [12] G.I. Barenblatt and L.R. Botvina, in: *Proceedings of Int. Symposium on Defects and Fracture*, edited by Sih and Zorski, Martin Nijhoff, Boston, pp. 71-79 (1982)
- [13] J.P.B. Leite, V. Slowik and H. Mihashi: *Cement Concrete Res.* Vol. 34 (2004), pp. 1025-1033